Enhanced Levels of microRNA-125b in Vascular Smooth Muscle Cells of Diabetic *db/db* Mice Lead to Increased Inflammatory Gene Expression by Targeting the Histone Methyltransferase Suv39h1

Louisa M. Villeneuve, Mitsuo Kato, Marpadga A. Reddy, Mei Wang, Linda Lanting, and Rama Natarajan

OBJECTIVE—Diabetes remains a major risk factor for vascular complications that seem to persist even after achieving glycemic control, possibly due to "metabolic memory." Using cultured vascular smooth muscle cells (MVSMC) from type 2 diabetic *db/db* mice, we recently showed that decreased promoter occupancy of the chromatin histone H3 lysine-9 methyltransferase Suv39h1 and the associated repressive epigenetic mark histone H3 lysine-9 trimethylation (H3K9me3) play key roles in sustained inflammatory gene expression. Here we examined the role of microRNAs (miRs) in Suv39h1 regulation and function in MVSMC from diabetic mice.

RESEARCH DESIGN AND METHODS—We used luciferase assays with Suv39h1 3′untranslated region (UTR) reporter constructs and Western blotting of endogenous protein to verify that miR-125b targets Suv39h1. We examined the effects of Suv39h1 targeting on inflammatory gene expression by quantitative real time polymerase chain reaction (RT-qPCR), and H3K9me3 levels at their promoters by chromatin immunoprecipitation assays.

RESULTS—We observed significant upregulation of miR-125b with parallel downregulation of Suv39h1 protein (predicted miR-125b target) in MVSMC cultured from diabetic *db/db* mice relative to control *db/+*. miR-125b mimics inhibited both Suv39h1 3′UTR luciferase reporter activity and endogenous Suv39h1 protein levels. Conversely, miR-125b inhibitors showed opposite effects. Furthermore, miR-125b mimics increased expression of inflammatory genes, monocyte chemoattractant protein-1, and interleukin-6, and reduced H3K9me3 at their promoters in nondiabetic cells. Interestingly, miR-125b mimics increased monocyte binding to *db/+* MVSMC toward that in *db/db* MVSMC, further imitating the proinflammatory diabetic phenotype. In addition, we found that the increase in miR-125b in *db/db* VSMC is caused by increased transcription of miR-125b-2.

CONCLUSIONS—These results demonstrate a novel upstream role for miR-125b in the epigenetic regulation of inflammatory genes in MVSMC of *db/db* mice through downregulation of Suv39h1.***Diabetes*** **59:2904–2915, 2010**

From the Department of Diabetes, Beckman Research Institute of City of Hope, Duarte, California.

Corresponding author: Rama Natarajan, RNatarajan@coh.org.

Received 10 February 2010 and accepted 13 July 2010. Published ahead of print at http://diabetes.diabetesjournals.org on 10 August 2010. DOI: 10.2337/db10-0208.

Diabetes is associated with increased risk for cardiovascular complications related to vascular inflammation and atherosclerosis (1–2). Hyperglycemia has been implicated in several diabetic complications via the activation of key signaling pathways leading to inflammatory gene expression (2–10). Increased levels of inflammatory cytokines and chemokines such as interleukin-6 (IL-6) and monocyte chemoattractant protein-1 (MCP-1) have been associated with diabetic complications and insulin resistance (2,4,10). Chronic inflammation and lipid accumulation in the arterial walls lead to monocyte/macrophage recruitment as well as vascular smooth muscle cell (VSMC) migration and proliferation to promote atherosclerosis (1,11), and these events are further accelerated in diabetes. Although it is known that inflammatory genes play key roles in the progression of atherosclerosis and diabetic complications, much less is known about the mechanism of their regulation especially at the level of chromatin or microRNAs.

Gene expression is regulated by active and repressed states of chromatin which rely not only on transcription factor binding, but also on the recruitment of protein complexes that change chromatin structure through epigenetic post-translational modifications of histone tails such as acetylation, phosphorylation, ubiquitination, and methylation. Furthermore, histone lysine (K) residues can be mono-(me1), di-(me2), or tri-(me3) methylated at various positions depending on the specificity of the histone methyl transferase (HMT) (12). Histone H3K9me3 can be mediated by the mammalian homologs of the *Drosophila* suppressor of position effect variegation, SUV39H1 in humans and Suv39h1 in mice, and plays an important role in heterochromatic silencing (13). Reports also show a role for SUV39H1 and H3K9me3 in euchromatic transcriptional repression (14). Changes in H3K9me have also been identified at the promoters of inducible inflammatory genes in monocytes and dendritic cells (15–16).

Clinical studies (17–20) have shown that prior conventional versus intensive glycemic control can leave a metabolic or transcriptional memory on target cells that lead to sustained long-term complications even after attainment of normoglycemia. We recently showed that VSMC cultured from the aortas of type 2 diabetic *db/db* mice (cultured vascular smooth muscle cells [MVSMC]) displayed a preactivated phenotype with enhanced inflammatory gene expression and proatherogenic responses relative to MVSMC from genetic control *db/+* mice, even

after in vitro culture for several passages, thereby mimicking metabolic memory of sustained vascular dysfunction in this model (21–22). Further studies showed that epigenetic chromatin histone lysine methylation on inflammatory gene promoters was altered in MVSMC from *db/db* mice. Thus, there was decreased repressive histone H3 lysine-9 trimethylation mark (H3K9me3) at the promoters of upregulated inflammatory genes in *db/db* MVSMC relative to control *db/+* (22). Histone lysine methylation at several loci, including inflammatory genes, was also altered in VSMC and monocytes cultured in high glucose (22–23). Two other reports have implicated histone H3 lysine-4 methylation with increased NF-κB and inflammatory gene expression and hyperglycemic memory in endothelial cells (24–25). We also demonstrated that Suv39h1 protein occupancy was reduced in parallel with the decreased H3K9me3 levels at the promoters of upregulated inflammatory genes in response to an inflammatory stimulus in cultured *db/db* MVSMC relative to *db/+* cells even after several passages in vitro, suggesting a potential role for Suv39h1 dysregulation in this model of metabolic memory (22). Although this evidence supports a dynamic role for Suv39h1 and H3K9me3 in inflammatory gene expression, the mechanism of Suv39h1 regulation itself under these diabetic conditions is unclear and was therefore investigated in this study.

MicroRNAs (miRs) pose an exciting emerging area of research because of their involvement in diverse biologic processes. The miRs are short noncoding RNAs (21–25 nucleotides in length) that can negatively regulate gene expression. Most mammalian miRs bind to the 3′untranslated regions (UTRs) of target mRNA transcripts leading to post transcriptional and translational repression, mRNA cleavage or degradation (26–27). Numerous miRs have been identified or predicted; however, their cellular targets, biologic roles and disease relevance are still under investigation. miRs have been found to play key roles in carcinogenesis (28), development, differentiation, fat metabolism, and insulin secretion (26–29). In VSMC, key miRs such as miR-21, miR-143, miR-145, and miR-221 have recently been shown to play important roles in phenotypic changes, migration, proliferation, and neointimal thickening (30–34). Key miRs such as miR-192, miR-216, and miR-377 were upregulated in renal cells leading to increased collagen and fibronectin expression associated with the pathogenesis of diabetic nephropathy (35–38). Evidence also shows miR targeting of a histone lysine methyltransferase EZH2 that mediates H3K27me3 involved in skeletal muscle differentiation (39), thereby suggesting a role for miRs in chromatin remodeling.

In the current study, we evaluated whether miRs might play a role in the dysregulation of Suv39h1 and associated chromatin H3K9me3 related to the increased expression of inflammatory genes observed in MVSMC of diabetic *db/db* mice (22). We report that, relative to control *db+* mice, MVSMC cultured from diabetic *db/db* mice express higher levels of miR-125b along with key inflammatory genes, but reciprocally express lower levels of the H3K9 HMT Suv39h1, a target of miR-125b. Downregulation of Suv39h1 by miR-125b led to derepression of key inflammatory chemokines and cytokine genes in nondiabetic cells via decrease of the repressive H3K9me3 chromatin mark at their promoters, suggesting that miR-125b can promote a diabetic phenotype. Thus, we have identified, for the first time, a miR-dependent mechanism for reduced Suv39h1 and associated epigenetic mechanisms underlying the increased inflammatory gene expression in the MVSMC of type 2 diabetic mice. These results reveal a previously uncharacterized miR-chromatin cross-talk mechanism for inflammatory gene expression related to sustained diabetic complications.

RESEARCH DESIGN AND METHODS

Materials. Antibodies against H3K9me1 (07-450), H3K9me2 (07-441) and H3K9me3 (07-442), and SUV39H1 (05-615) were from Millipore (Billerica, MA). In some experiments (Fig. 1*B*), SUV39H1 rabbit polyclonal antibody (ARP32470 T100) from Aviva Systems (San Diego, CA) was used. The β-actin antibody was from Santa Cruz Biotech (Santa Cruz, CA). The SYBR Green PCR Master Mix kit was from Applied Biosystems (Foster City, CA). RNA-STAT 60 was from Iso-Tex Diagnostics (Friendswood, TX). The miR-125b mimic, inhibitors, and negative controls oligonucleotides were from Dharmacon RNAi Technologies (Lafayette, CO). FLAG-SUV39H1 plasmid vector was previously described (22). Fluorescent dye 2′,7′-Bis-(2-carboxyethyl)-5-(and 6)-carboxyfluorescein acetoxymethyl ester (BCECF/AM) was from A.G. Scientific (San Diego, CA).

Cell culture. All animal studies were performed according to protocols approved by the Institutional Animal Care and Use Committee. Mouse vascular smooth muscle cells (MVSMC) were isolated from thoracic aortas of 10- to 12-week-old male diabetic (average blood glucose levels >450 mg/dl) *db/db* mice (BKS.Cg-m+/+leprdb/J, Jackson Laboratory, Bar Harbor, ME), and heterozygous nondiabetic *db/+* control littermates, as previously described (21–22). MVSMC were cultured in Dulbecco's modified Eagle's medium (DMEM)/F12 medium supplemented with 10% FBS for 5 to 8 weeks. During this period, the *db/db* cells continued to maintain the diabetic phenotype relative to *db/+* cells (21–22). Mouse kidney epithelial cells TCMK-1 (38) and HeLa (ATCC # CCL2) cells were cultured in DMEM supplemented with 10% FBS. WEHI78/24 cells (21–22) were cultured in DMEM containing 10% heat-inactivated FBS.

Immunohistochemistry. Formalin fixed, paraffin-embedded sections of *db/+* and *db/db* mouse aortas were deparaffinized in xylene followed by 100% ethanol. Quenching in 3% hydrogen peroxide was followed by pretreatment with steam in DIVA/citrate buffer (pH 6.0) solution to promote antigen retrieval. Slides were then incubated in Rodent Block-M for 30 min followed by 30 min with SUV39H1 antibody (1:15) in Dako dilution buffer. Slides were then washed in Dako wash buffer and incubated for 20 min in MM polymer-HRP (horseradish peroxidase) followed by incubation with the chromogen diaminobenzidine tetrahydrochloride (Dako DAB) for 10 min, counterstained with hematoxylin, and mounted. Images were taken at ×40 magnification using an Olympus BX51 microscope with InStudio (Pixera Corp) software to collect images and ImagePro software (Media Cybernetics, MD) to quantify staining.

Chromatin immunoprecipitation assays. Cells were fixed with 1% formaldehyde and chromatin immunoprecipitation (ChIP) assays with cell lysates using indicated antibodies were performed as previously described (22). ChIP-enriched DNA samples were analyzed by quantitative polymerase chain reaction (qPCR) with primers surrounding NF-κB binding sites in the indicated gene promoters (data are available in supplemental Table S1, available online at http://diabetes.diabetesjournals.org/cgi/content/full/db10-0208/DC1), data analyzed using the $2^{-\Delta\Delta CT}$ method, normalized with input samples, and results expressed as a percentage of control as described earlier (22).

Western blotting and quantification. Immunoblotting was performed as previously described (40). Briefly, equal amounts of cell lysates were run on 10% denaturing PAGE gels and transferred to nitrocellulose membrane. Membranes were blocked, incubated with primary antibody, washed, and incubated with appropriate HRP-conjugated secondary antibody. Membranes were again washed and protein bands visualized using an enhanced chemiluminescence kit (PerkinElmer, Waltham, MA). Contrast was adjusted uniformly across the whole autoradiogram to better visualize the bands. Intensity of protein bands was quantified using a calibrated densitometer GS-800 and Quantity One software (Bio-Rad, Hercules, CA).

miR-125b quantification. Levels of miR-125b were determined by quantitative real time polymerase chain reaction (RT-qPCR) as described previously (37,38). Primer sequences are provided in online supplemental Table S1. Amplification of a single fragment was verified with a single peak in the dissociation curve, and mean quantity was determined based on a standard curve amplified by a known template. As an internal control, 5S RNA (Ambion) was used ($n = 3$). To confirm results, miScript system was used with miScript Reverse Transcription Kit and a miScript SYBR Green PCR Kit (Qiagen, Valencia, CA) for detection of mature miR-125b using primers specific for miR-125b according to the manufacturer's protocols ($n = 4$).

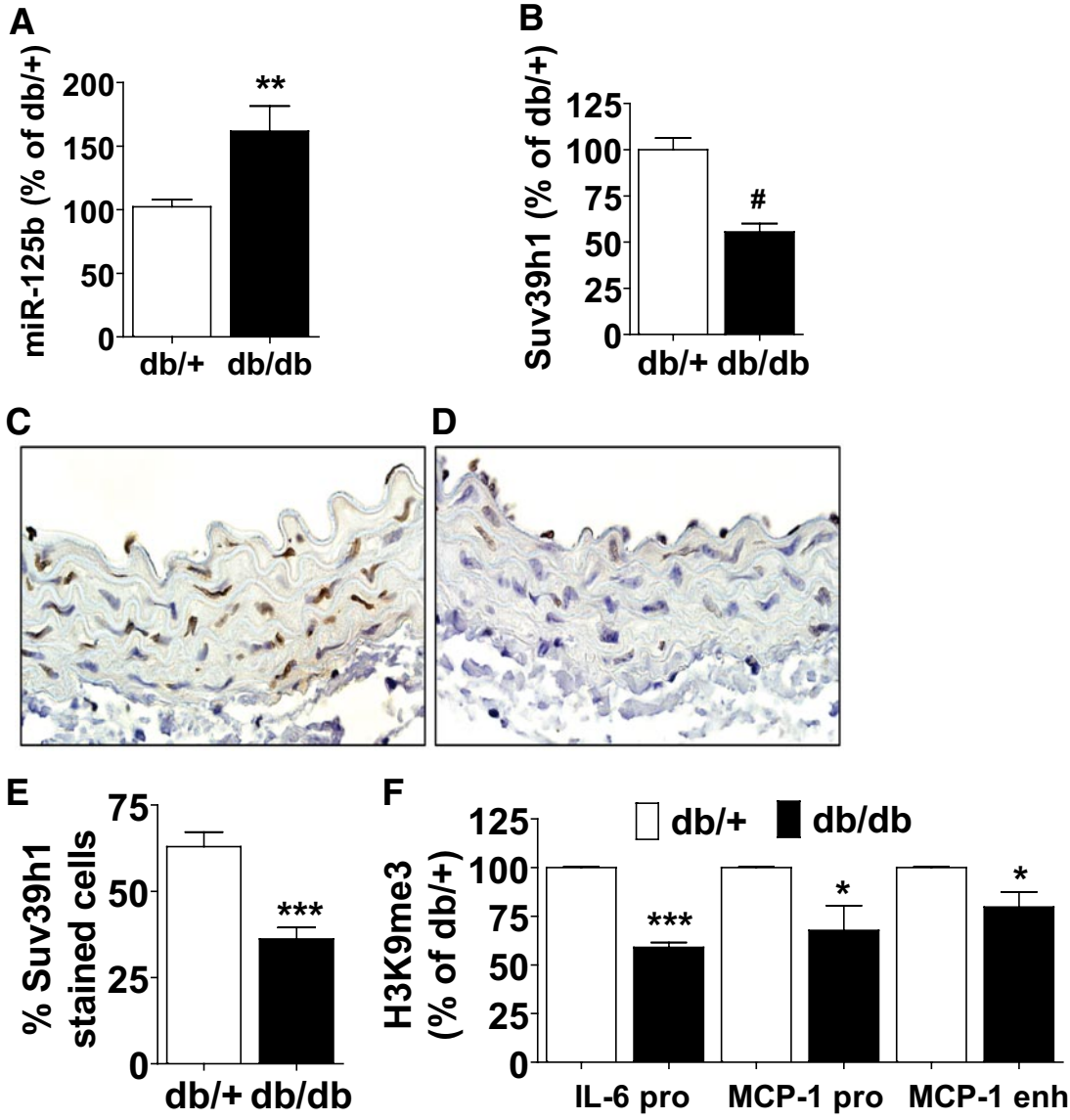

FIG. 1. Upregulation of miR-125b, decrease in Suv39h1 expression, and decrease in inflammatory gene promoter H3K9me3 levels in diabetic VMSC. *A*: The miR-125b levels in cultured MVSMC from *db/+* and *db/db* mice were analyzed by RT-qPCR and results expressed as the percentage of *db/+* (mean ± SEM, **$P < 0.01$, $n = 7$). *B*: Quantification of Suv39h1 protein levels from MVSMC cell lysates immunoblotted with Suv39h1 antibodies. Results expressed as the percentage of db/+ (#, $P < 0.001$, $n = 3$). *C* and *D*: Representative aortic sections from *db/+* (*C*) and *db/db* (*D*) mice stained with SUV39H1 antibody (brown) and nuclear stain hematoxylin (blue) (×40 magnification). *E*: Suv39h1-stained MVSMC nuclei from (*C* and *D*) were counted, and results expressed as the percentage of nuclei stained with Suv39h1 (mean ± SE, ***$P < 0.0001$ vs. *db/+*, $n = 3$). *F*: H3K9me3 levels determined by ChIP assays. ChIP enriched DNA samples analyzed by qPCR using indicated promoter (pro) or enhancer (enh) primers. Results expressed as the percentage of *db/+* (*$P < 0.05$; ***$P < 0.0001$, $n = 3$ for IL-6, and $n = 4$ for MCP-1 promoter and enhancer). (A high-quality color representation of this figure is available in the online issue.)

Construction of Suv39h1 3′UTR reporters. Suv39h1 3′UTR containing potential miR-125b target sequence was amplified by PCR and subcloned downstream of luciferase gene (in *Not*I site) of psiCHECK-2 dual luciferase vector (Promega, WI) in both sense (Suv39h1 S-3′UTR) and antisense (Suv39h1 AS-3′UTR) orientations. Primers used for amplification were 5′-GGCCCATACAGATTGTCTCAGGGA-3′ (sense); and 5′-GGCCTCCCTGAGA CAATCTGTATG-3′ (antisense). Similar strategy was used to clone PPARα 3′UTR into psiCHECK-2 vector (sense, 5′-GGCCTAAAGAGTTAATT TCAGGGT-3′; AS, 5′-GGCCACCCTGAAATTAACTCTTTA-3′).

Transfections and luciferase assays. MVSMC were transfected with indicated plasmids/oligos using the Nucleofection method (Lonza) as previously described (22). TCMK-1 and HeLa cells were transfected using X-tremeGENE (Roche) according to the manufacturer's protocols. Transfected cells were harvested 24–48 h after transfection for various assays as indicated. To examine the luciferase activity of 3′-UTR constructs, TCMK-1 cells were cotransfected with 10 nmol/l of miR-125b mimic or negative control (NC) oligonucleotides along with 100 ng of indicated 3′-UTR reporter constructs. MVSMCs were cotransfected with 25 nmol/l of miR-125b mimic or 5 nmol/l of inhibitor hairpins or the respective negative controls along with 1 μg of 3′-UTR reporter constructs. Cells were harvested 48 h after transfection and luciferase activities in cell lysates determined with the Dual-Luciferase Assay System (Promega) using TD20/20 luminometer (Turner Designs) or Veritas microplate luminometer (Turner BioSystems) according to the manufacturer's protocols.

RT-qPCR to quantify gene expression. Total RNA was extracted using RNA-STAT60 and reverse transcription followed by RT-qPCR used to measure inflammatory gene expression levels using β-actin as an internal control as described before (22). Primer sequences are provided in online supplemental Table S1.

Monocyte binding assays. Monocyte binding assays were performed as previously described (21) with some modifications. MVSMC (5×10^5 cells) were transfected by Nucleofection with indicated oligonucleotides/plasmids and plated in quadruplicate in 24-well plates. After 48 h, MVSMC monolayers were incubated with WEHI78/24 mouse monocytic cells (6×10^4/well) fluorescently labeled with BCECF/AM (10 μg/ml), for 1 h at 37°C. Nonspecifically-bound monocytes were removed by gently washing monolayers 4 to 5

times with DMEM containing 0.5% FBS. Fluorescent images (3 to 4 fields per well) of bound monocytes were taken at ×10 magnification using an Olympus IX50 microscope and Olympus Microsuite software. The numbers of bound monocytes were counted using AlphaEaseFC software (Cell Biosciences, Santa Clara, CA).

Statistics. We used PRISM software (Graph-Pad) for data analysis with Student *t* tests or ANOVA. $P < 0.05$ was considered statistically significant. Data are expressed as means ± SE.

RESULTS

Upregulation of miR-125b in diabetic *db/db* mice. To identify previously uncharacterized roles of miRs in the increased vascular inflammation in diabetes, we screened for miRs that were differentially expressed in total RNA obtained from various cells of diabetic *db/db* versus genetic control *db/+* mice. Initial miR microarray profiling identified miR-125b as being upregulated in *db/db* mice (unpublished observations). These results were verified by RT-qPCR, which revealed a significant increase in miR-125b levels in MVSMC cultured from diabetic *db/db* mice relative to control *db/+* (Fig. 1*A*). The cultured diabetic MVSMC also expressed a persistent increase in the expression of inflammatory genes such as *MCP-1* and *IL-6*, as previously shown (21–22). Since these MVSMC had been cultured for several passages outside the diabetic animal, the sustained increase in miR-125b in the diabetic *db/db* cells relative to *db/+* cells suggests a potential memory of dysregulated miR-125b expression.

Potential targets of miR-125b. Using computational miR target predictions from miR databases, including MIRANDA (http://cbio.mskcc.org), MiRBase Targets (http://microrna.sanger.ac.uk/targets/v4), and TargetScan (http://www.targetscan.org/vert_42), we identified the 3′UTR of Suv39h1 as a potential target of miR-125b. The Suv39h1–3′UTR has a perfect match to the miR-125b seed region and is conserved between human, rat, and mouse (online supplemental Fig. S1A).

Decreased Suv39h1 expression in diabetic *db/db* MVSMC and parallel decrease in H3K9me3 at inflammatory gene promoters inversely correlates with miR-125b. We recently demonstrated that reduced H3K9me3 and recruitment of Suv39h1 at inflammatory gene promoters was a key mechanism underlying the enhanced inflammatory gene expression in *db/db* MVSMC (22). We therefore hypothesized that, under diabetic conditions, upregulation of miR-125b can enhance the expression of key inflammatory genes by downregulating its target Suv39h1 with concomitant reduction in H3K9me3 levels (repressive mark) at the promoters of these genes associated with vascular dysfunction. To test this, we next evaluated whether increased miR-125b inversely correlated with the expression of its potential target, Suv39h1, in the diabetic MVSMC. Immunoblotting showed that Suv39h1 protein levels were decreased by 45% in cultured *db/db* MVSMC relative to *db/+* (Fig. 1*B*), as also noted previously (22). Interestingly, immunohistochemistry also revealed a significant decrease in nuclear Suv39h1 protein levels in MVSMC regions of aortic sections from *db/db* mice compared with *db/+* (Fig. 1*C–E*), demonstrating in vivo relevance. Furthermore, ChIP assays showed a significant decrease in H3K9me3 levels at the IL-6 and MCP-1 promoters and MCP-1 enhancer in *db/db* MVSMC relative to *db/+* (Fig. 1*F*). These results demonstrate that miR-125b levels inversely correlate with Suv39h1 levels, suggesting a novel mechanistic basis for the decreased Suv39h1 and reduced H3K9me3 levels associated with the reciprocal increase in *IL-6* and *MCP-1* expression in the *db/db* MVSMC which persisted even after in vitro culture for several passages. Interestingly, there were no changes in global levels of total H3K9me3, H3K9me2, or H3K9me1 (online supplemental Fig. S2), suggesting specificity and that increased miR-125b in *db/db* cells affects H3K9me3 only at a subset of gene promoters, but not total H3K9me3.

Suv39h1 3′UTR is a true target of miR-125b. Next, to verify that the 3′UTR of Suv39h1 was indeed an actual target of miR-125b, we examined the effects of a double-stranded RNA oligonucleotide mimicking the mature miR-125b (mimic) on luciferase activity of reporters containing the Suv39h1 3′UTR downstream of luciferase gene in sense (S-3′UTR) or antisense (AS-3′UTR) orientations. In TCMK-1 cells, miR-125b mimic significantly decreased luciferase activity of the Suv39h1 S-3′UTR reporter compared with negative control oligonucleotides for the mimic (NC-M) derived from a *C. elegans* sequence (Fig. 2*A*). In contrast, miR-125b mimic had no effect on either Suv39h1 AS-3′UTR or the psiCHECK-2 vector alone (Fig. 2*A*). Furthermore, miR-125b did not inhibit the luciferase activity of a reporter containing the 3′-UTR of peroxisome proliferator activated receptor-α (PPARα) which also has a putative miR-125b binding site (Fig. 2*B*, and supplemental Fig. S1*B*), thus demonstrating specificity of Suv39h1 3′UTR targeting by miR-125b.

Targeting of Suv39h1 3′UTR by miR-125b was next tested in primary MVSMC derived from control *db/+* mice. Interestingly, luciferase activity of Suv39h1 S-3′UTR transfected with NC-M oligo was decreased relative to empty psiCHECK-2 vector (control) transfected with NC-M (Fig. 2*C*), most likely caused by endogenous levels of miR-125b in *db/+* cells. Furthermore, luciferase activity of the S-3′UTR (but not control or AS) was further decreased when cotransfected with miR-125b mimic (Fig. 2*C*). Since our data showed that diabetic *db/db* MVSMC display higher levels of endogenous miR-125b compared with *db/+*, we next examined the activity of Suv39h1 S-3′UTR construct in both *db/+* and *db/db* MVSMC cells. Results showed that Suv39h1 S-3′UTR activity was significantly lower in *db/db* MVSMC compared with *db/+*, demonstrating that higher endogenous miR-125b in *db/db* cells can result in enhanced targeting (Fig. 2*D*).

We next tested whether, reciprocally, an inhibitor of miR-125b could reverse these effects. We used two hairpin inhibitors designed to interfere with miR incorporation into the RISC complex, thereby preventing targeting of the mRNA transcript. Results showed a decrease in luciferase activity of Suv39h1 S-3′UTR relative to Suv39h1 AS-3′UTR in MVSMC transfected with a negative control hairpin for the inhibitors (NC-I) derived from a *C. elegans* sequence (Fig. 2*E*), most likely caused by endogenous miR-125b. Moreover, this decrease was partially but significantly reversed by cotransfection with either miR-125b inhibitor Inh.1 or Inh.2 (Fig. 2*E*) with no effect on the control AS-3′UTR. Thus, inhibition of miR-125b blocks the targeting of Suv39h1 3′UTR, resulting in increased luciferase activity. Together, these results further confirm that Suv39h1 3′UTR is targeted by miR-125b.

miR-125b mimic downregulates endogenous Suv39h1. We next examined whether transfection of miR-125b mimic can induce a diabetic phenotype of decreased Suv39h1 in control *db/+* MVSMC. Both *Suv39h1* mRNA levels (Fig. 3*A*) and protein levels (Fig. 3*B*) were

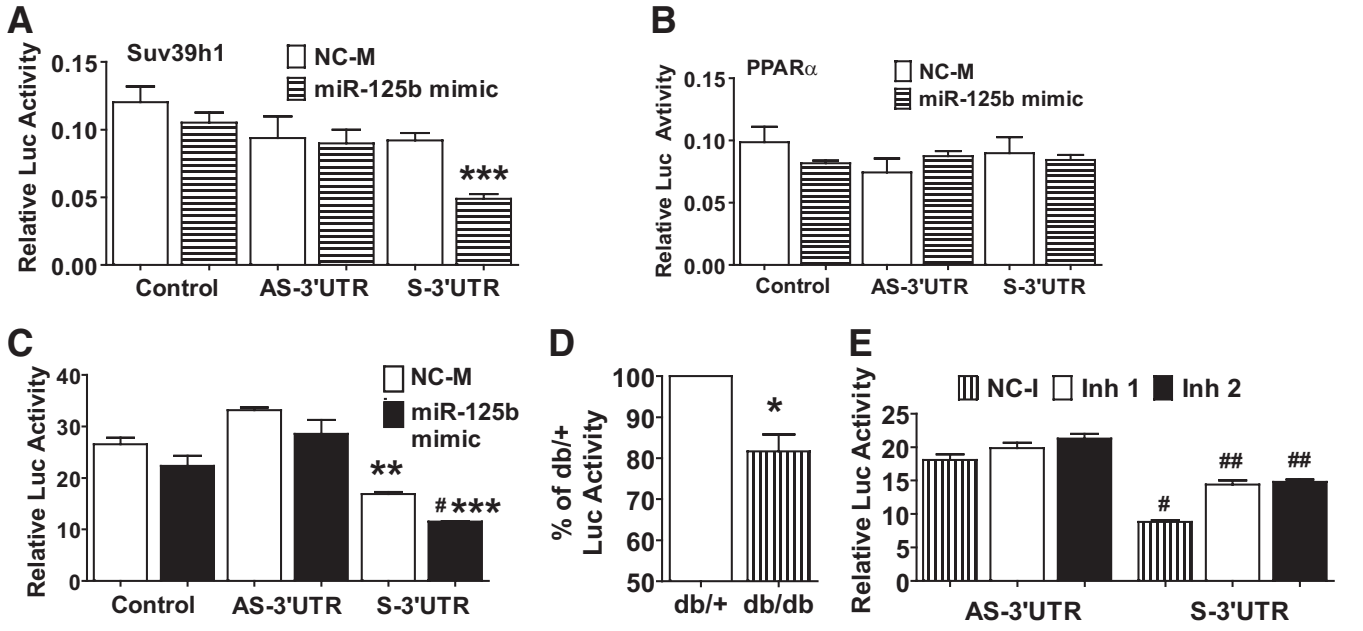

FIG. 2. Suv39h1 3′UTR is a true target of miR-125b. *A* and *B*: Luciferase activity of TCMK-1 cells cotransfected with empty vector (control) or with SUV39h1–3′UTR (*A*) or PPARα-3′UTR (*B*) in sense (S-3′UTR) or antisense orientation (AS-3′UTR), along with miR-125b mimic or negative control for the mimic (NC-M) oligonucleotides (*$P < 0.0001$ vs. NC-M S-3′UTR, $n = 3$). *C*: Relative luciferase activity in *db/+* MVSMC cotransfected with the indicated vectors along with miR-125b mimic or NC-M oligonucleotides (**$P < 0.01$; #$P < 0.001$ vs. NC-M control or AS-3′UTR by ANOVA; and ***$P < 0.0001$ vs. NC-M S-3′UTR by Student *t* test, $n = 3$). *D*: Effect of endogenous miR-125b in *db/db* vs. *db/+* MVSMC transfected with Suv39h1 S-3′UTR reporter. Luciferase activity was expressed as the percentage of *db/+* (*$P < 0.05$, $n = 3$). *E*: Relative luciferase activity of *db/+* MVSMC cotransfected with Suv39h1 AS-3′UTR or S-3′UTR along with miR-125b inhibitors or negative control for the inhibitors (NC-I) (#$P < 0.0001$ vs. AS-3′UTR NC-I; and, ##$P < 0.0001$ vs. S-3′UTR NC-I, $n = 3$).**

significantly decreased in *db/+* cells toward that seen in *db/db* cells after transfection with the miR-125b relative to NC-M.

We next tested whether, conversely, miR-125b-specific inhibition can reverse the targeting of Suv39h1 and diabetic phenotype of *db/db* MVSMC. Transfection of *db/db* MVSMC with miR-125b inhibitor hairpins Inh.1 or Inh.2, or mixture of both, significantly increased *Suv39h1* mRNA (Fig. 3*C*) and protein levels (Fig. 3*D*) compared with NC-I. Neither the miR-125b mimic nor inhibitors had any effect on glyceraldehyde 3-phosphate dehydrogenase (GAPDH) housekeeping gene levels in MVSMC (Fig. 3*E–F*) demonstrating specificity. These results demonstrate that miR-125b addition to normal cells can mimic, at least in part, the diabetic phenotype by decreasing endogenous Suv39h1, whereas, in contrast, miR-125b inhibitors reverse these effects in diabetic cells.

miR-125b mediated knockdown of SUV39H1 leads to decreased promoter H3K9me3 and increased inflammatory gene expression. We next evaluated whether miR-125b mediated knockdown of Suv39h1 can functionally decrease H3K9me3 at the promoters of inflammatory genes with a parallel increase in their expression. HeLa cells were used here because of the need for high transfection efficiency for the subsequent assays. HeLa cells were transfected with miR-125b mimic or NC-M, and processed for various assays 24 h later. Immunoblotting of cell lysates confirmed a significant decrease in endogenous human SUV39H1 protein levels in cells transfected with miR-125b mimic relative to NC-M (Fig. 4*A* and *B*) demonstrating that miR-125b targeting of SUV39H1 can occur in multiple cell types. ChIP assays showed that miR-125b mimic significantly decreased the repressive mark H3K9me3 at the IL-6 and MCP-1 promoters and MCP-1 enhancer (Fig. 4*C*) and reciprocally increased *IL-6* and *MCP-1* mRNA expression (Fig. 4*D* and *E*). The miR-125b mimic had no significant effect on H3K9me3 levels at the promoters of housekeeping genes GAPDH or cyclophilin A (CYPA), or on their expression levels (online supplemental Fig. S3*A* and *B*) demonstrating specificity and that only a subset of genes are regulated by Suv39h1. The specificity of miR-125b was further evident from ChIP data showing that miR-125b mimic did not affect either H3K9me1 or H3K9me2 levels at the IL-6, MCP-1, CYPA and GAPDH promoters, or MCP-1 enh in HeLa cells (online supplemental Fig. S4*A* and *B*). In addition,Western blots showed that miR-125b mimic clearly decreased global levels of only total H3K9me3, but not global H3K9me1 or H3K9me2 (online supplemental Fig. S5).

To further verify the role of miR-125b targeting SUV39H1 in leading to increased inflammatory gene expression, we examined whether SUV39H1 overexpression can reverse the increased inflammatory gene expression induced by exogenous miR-125b. HeLa cells were cotransfected with miR-125b mimic or NC-M, along with control empty vector pCR3.1 (pCR) or FLAG-SUV39H1 (pSUV) expression vector, which does not contain the SUV39H1 3′UTR (i.e., no miR-125b seed sequence). Cotransfection of miR-125b mimic with control pCR-induced inflammatory gene expression similar to that seen in miR-125b mimic transfected cells (Fig. 4*D* and *E*). However, miR-125b mimic-induced expression of *IL-6* and *MCP-1* was clearly attenuated in pSUV cotransfected cells relative to pCR (Fig. 4*F*). No significant changes were seen in CYPA expression (supplemental Fig. S3*C*) under these conditions. These results further support the notion that decreased SUV39H1 and promoter H3K9me3 are associated with a corresponding upregulation of certain inflammatory genes similar to

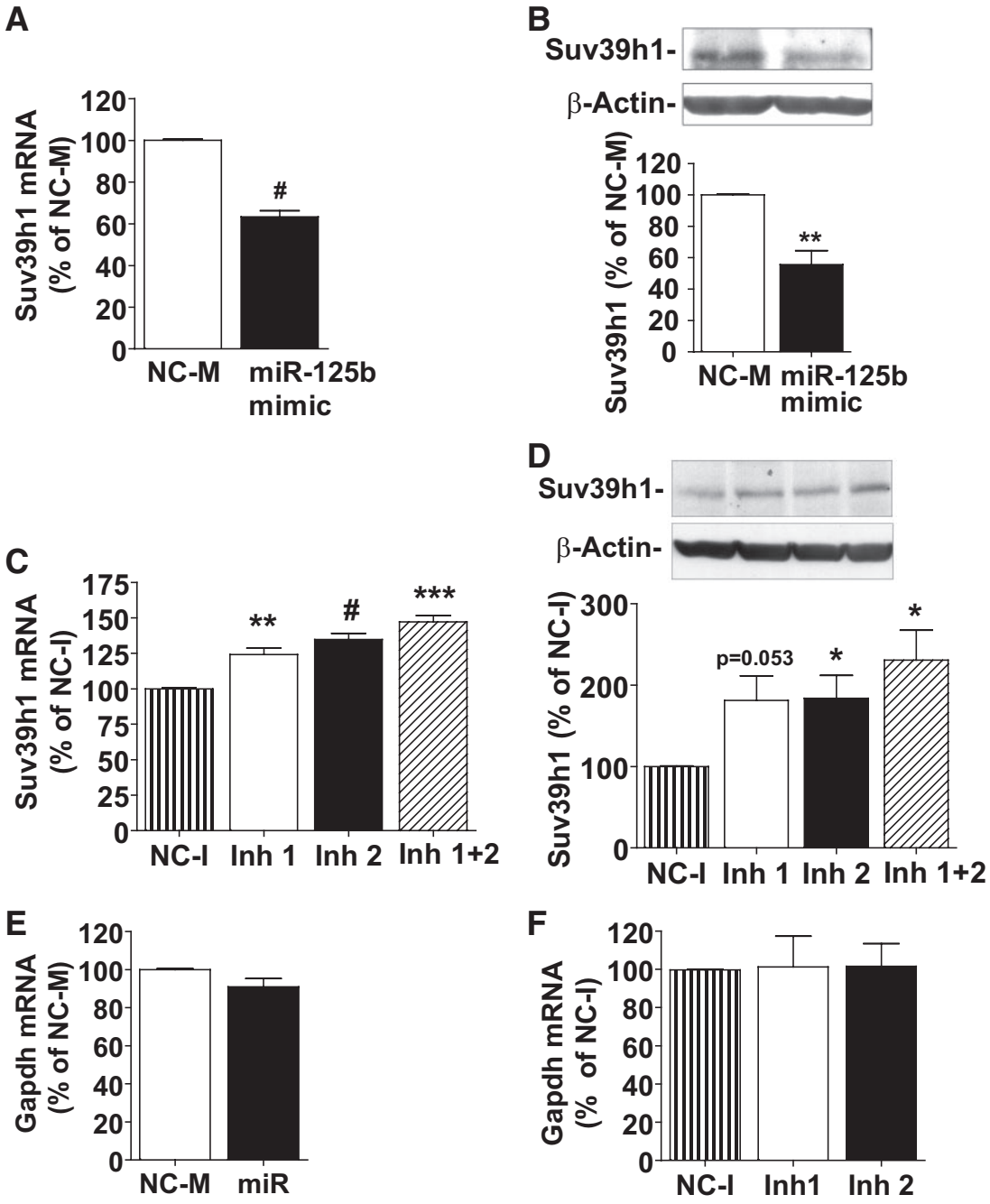

FIG. 3. Regulation of endogenous Suv39h1 mRNA and protein levels by miR-125b. *A* and *B*: Inhibition of Suv39h1 mRNA (*A*) and protein (*B*) levels in *db/+*MVSMC transfected with miR-125b mimic. *C* and *D*: Increased expression of Suv39h1 mRNA (*C*) and protein (*D*) by miR125b inhibitors 1 and 2 in *db/db* MVSMC. There was no change in GAPDH mRNA in *db/+* MVSMC transfected with miR-125b mimic (*E*), or in *db/db* transfected with inhibitors (Inh) 1 and 2 (*F*). In all of the experiments, MVSMC were transfected with the indicated oligonucleotides or hairpin inhibitors using the Nucleofection method, and 48 h after transfection, cells were processed for isolation of RNA or preparation of cell lysates. The mRNA levels were determined by RT-qPCR and normalized with internal control β-actin. Suv39h1 protein levels in cell lysates were determined by immunoblotting with Suv39h1 followed by internal control β-actin antibodies and quantified by densitometric scanning of blots. All results were expressed as percentages of NC-M or NC-I (mean ± SE, *$P < 0.05$, **$P < 0.01$; #$P < 0.001$; ***$P < 0.0001$ vs. NCs, $n = 3$).

that seen in the diabetic phenotype, and that this can be reversed by SUV39H1 reconstitution. This novel miR-dependent regulation affects key disease related genes, such as *IL-6* and *MCP-1*, but not others tested, and can be attenuated by blocking miR-125b.

miR-125b increases monocyte-MVSMC binding mimicking the diabetic phenotype. Monocyte recruitment into the vessel wall plays a key role in atherosclerosis (11,41). Monocyte adhesion to VSMC can increase subendothelial monocyte retention, survival, and differentiation, key steps in the progression of atherosclerosis (42). Diabetic *db/db* MVSMC exhibit increased monocyte binding relative to *db/+* controls, which can be attributed to the increased expression of chemokines such as MCP-1 (21). Therefore, we next examined the functional relevance of our data by testing whether increased miR-125b and the subsequent targeting of Suv39h1 in the diabetic *db/db* MVSMC can increase monocyte recruitment. We examined monocyte binding to *db/+* MVSMC transfected with miR-125b mimic or

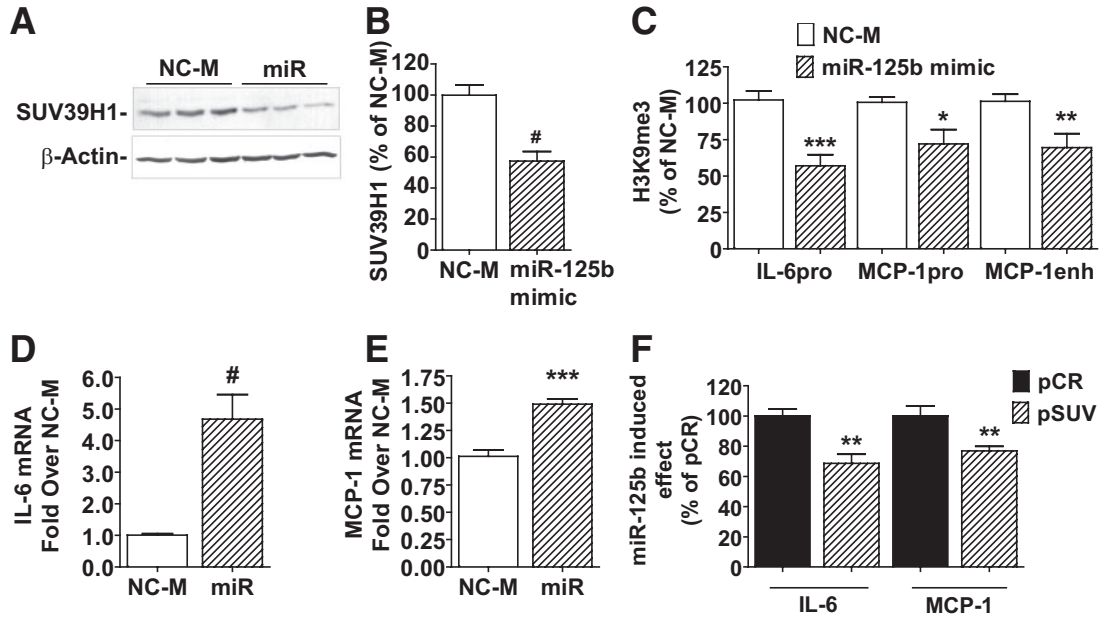

FIG. 4. The miR-125b mediated inhibition of SUV39H1 expression leading to decreased H3K9me3 and increased inflammatory gene expression. (*A–E*). Levels of SUV39H1 protein in cell lysates (*A* and *B*), H3K9me3 at inflammatory gene promoters (*C*), and inflammatory gene mRNAs (*D* and *E*) in HeLa cells transfected with miR-125b mimic or NC-M. HeLa cells were transfected with indicated oligonucleotides, and 24 h later, Suv39h1 protein levels determined by immunoblotting ($n = 3$), H3K9me3 levels at indicated genes (promoter = pro, and enhancer = enh) by ChIP-qPCRs ($n = 5$) and mRNAs by RT-qPCR ($n = 4$). Results are expressed as a percentage of NC-M (*B* and *C*) or fold over NC-M (*D* and *E*) (*$P < 0.05$; **$P < 0.01$; #$P < 0.001$; ***$P < 0.0001$ vs. NC-M). *F*: The miR-125b mimic or NC-M were transfected as in Fig. 4*D* and *E* along with either pCR3.1 empty vector (pCR) or FLAG-SUV39H1 (pSUV), incubated overnight, and gene expression analyzed by RT-qPCR. Results shown are the effects of miR-125b mimic on inflammatory genes in pSUV cotransfected cells relative to pCR (percentage of respective pCR control vector) ($P < 0.01$ vs. pCR, $n = 4$).**

NC-M. As a positive control, we used *db/db* MVSMC transfected with NC-M. As seen in Fig. 5, miR-125b mimic significantly increased monocyte binding to *db/+* MVSMC relative to NC-M, and this was similar to that in *db/db* cells transfected with NC-M (Fig. 5*A–C* and *G*). To further verify the role of Suv39h1 and whether augmenting Suv39h1 expression can reverse the diabetic phenotype, we performed monocyte-VSMC binding assays with *db/db* MVSMC transfected with FLAG-SUV39H1 lacking the 3′UTR (pSUV) and control pCR3.1 (pCR). Increasing SUV39H1 led to a small but significant attenuation in monocyte binding to *db/db* MVSMC (Fig. 5*D–F* and *H*). Although the increased monocyte binding in miR-125b mimic transfected *db/+* MVSMC was not the same as in *db/db* MVSMC with NC-M, and reconstituting SUV39H1 levels in *db/db* MVSMC only partially reversed the diabetic phenotype of enhanced monocyte-MVSMC adhesion, these changes were clearly significant, demonstrating that miR-125b plays a key, but not an exclusive role, in diabetes-induced monocyte recruitment into the vessel wall.

Increased transcriptional regulation of miR-125b in *db/db* cells. We next examined potential regulatory mechanisms for miR-125b in *db/db* MVSMC. The mouse genome has two copies of miR-125b, namely125b-1 and 125b-2, with both processed into the same mature miR (http://microrna.sanger.ac.uk/sequences) by enzymes such as Drosha and Dicer (26–27). The miR-125b-1 is located in the intron of a known protein coding transcript (2610203C20Rik-201) within chromosome 9, whereas miR-125b-2 is intergenic within chromosome 16 (Fig. 6*A*). Primers flanking the premiR-125b-1 sequence did not pick up any transcripts (not shown), suggesting that it is processed from the intron of 2610203C20Rik-201. Yet, RT-qPCR to amplify 2610203C20Rik-201 itself (primers p1-p2) indicated no change in its transcription in *db/db* MVSMC relative to *db/+* (Fig. 6*B*, left two bars). On the other hand, interestingly, RT-qPCR with primers flanking the premiR-125b-2 sequence (primers p3-p4) showed increased transcription of miR-125b-2 in *db/db* cells relative to *db/+* (Fig. 6*B*, right two bars).

We next verified the size of the miR-125b-2 transcript amplified with primers p3-p4 using conventional PCR followed by gel electrophoresis, and we detected a 240-base pair (bp) unprocessed pri-miR-125b-2 which was higher in *db/db* cells (Fig. 6*C* and *D*). Typically, pri-miRs are thought to be short lived in the nucleus and rapidly processed by Drosha into premiRs that are further processed into mature miRs by Dicer (26–27). However, we observed unprocessed pri-miR-125b-2 which was higher in *db/db* cells, suggesting increased transcriptional regulation of this region. Using the UCSC genome browser, we identified two cDNAs (AK039756 and AK047945 RIKEN full-length cDNA clones) that overlap with premiR-125b-2 (Fig. 6*A* right panel). RT-qPCR with primers p5-p6 designed to detect both AK039756 and AK047945, but downstream of premiR-125b-2, also revealed a significant increase in transcription in this region in *db/db* MVSMC relative to *db/+* (Fig. 6*E*).

We next performed PCRs with primers p3-p4 and p5-p6 to compare levels of the two transcripts. Both sets of primers demonstrated an approximately twofold increase in *db/db* MVSMC compared with *db/+* (Fig. 6*F*), but the absolute amount of transcript was greater with the latter set. These data suggest that miR-125b-2 may be transcribed along with the RIKEN cDNAs and then processed by Drosha and Dicer into the mature miR-125b. Since primers p3-p4 amplify only the residual unprocessed (uncropped) portion of the pri-miRNA, the levels detected are lower than the cDNA amplified with primers p5-p6 which

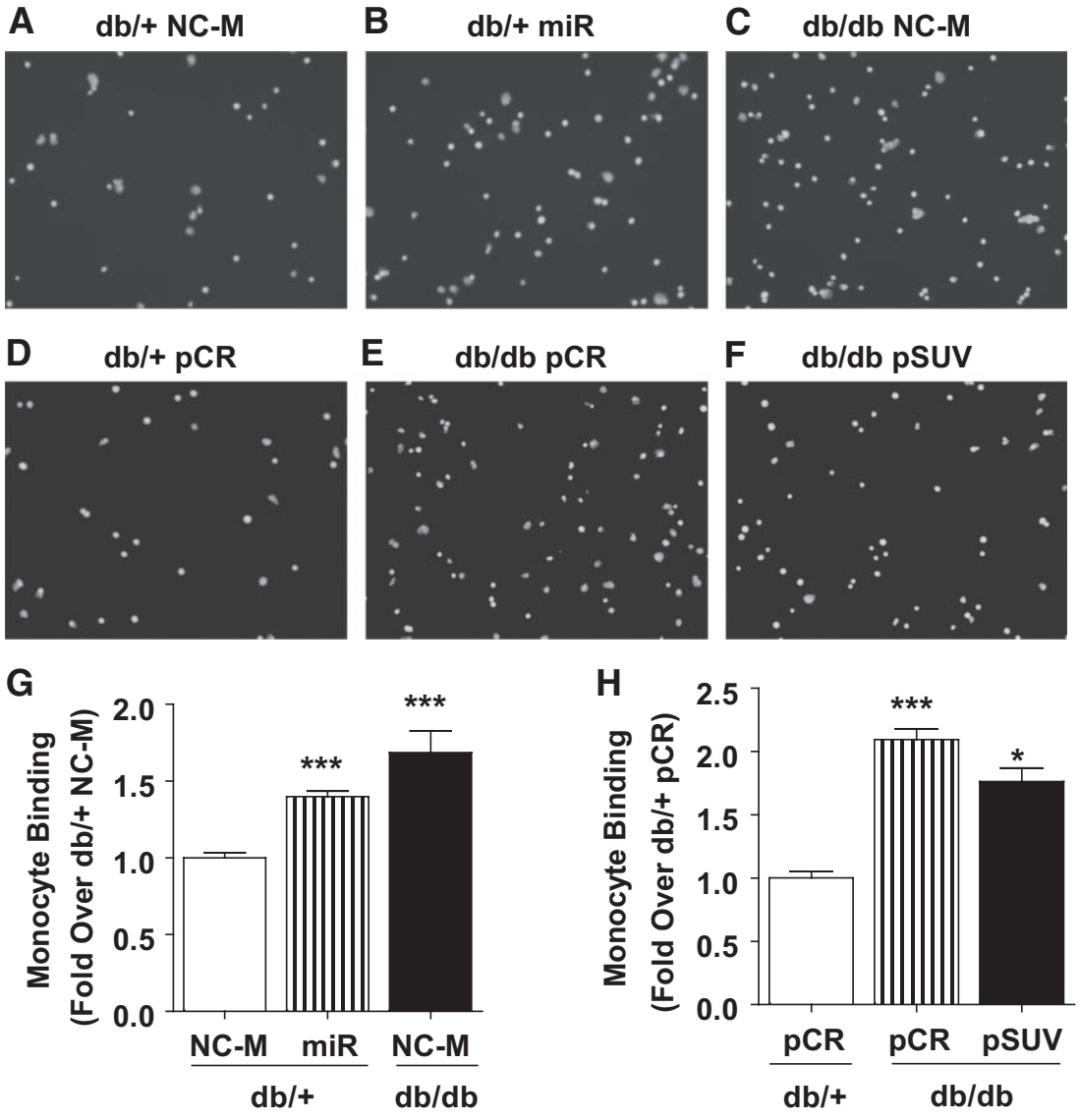

FIG. 5. The miR-125b and Suv39h1 regulate monocyte-MVSMC binding. MVSMC were transfected with indicated oligonucleotides or plasmids, and 48 h later, MVSMC-monocyte binding assays were performed by incubating with fluorescently labeled mouse WEHI78/24 monocytes. MVSMC monolayers were washed and images of bound monocytes collected at ×10 magnification using a fluorescence microscope. The number of bound monocytes were counted using AlphaEaseFC software (Alpha Innotech). *A–C*, *G*: MVSMC transfected with miR-125b mimic (miR) or NC-M. Results expressed as fold over *db/+* NC-M (*$P < 0.0001$ vs. NC-M, $n = 4$). *D–F*, *H*: MVSMC transfected with empty vector pCR3.1 (pCR) or FLAG-SUV39H1 (pSUV) expression vector. Results expressed as fold over pCR (***$P < 0.0001$ vs. *db/+* pCR or *$P < 0.05$ vs. *db/db* pCR, $n = 3$).**

detect the more stable portion of the primary transcript which is not affected by Drosha processing. To further verify these results, we performed RT-qPCR with primers p3-p6 to amplify this longer fragment containing miR-125b-2 along with the downstream sequence overlapping the RIKEN cDNA clones. Since this longer fragment was detectable (Fig. 6*G*), it likely constitutes a single transcript and premiR-125b-2 is cropped from this primary transcript. Interestingly, this was again increased approximately twofold in *db/db* MVSMC (Fig. 6*G*), suggesting increased transcription of any part of this region in *db/db* cells. Overall these results suggest that elevated levels of miR-125b are caused by increased transcriptional regulation of miR-125b-2 (and not miR-125b-1) in *db/db* relative to *db/+* MVSMC, and that miR-125b-2 may be processed from the longer primary transcript containing either AK039756 or AK047945 whose function is unknown to date.

DISCUSSION

In this study, we uncovered a novel miR-dependent mechanism for the epigenetic regulation of pathologic genes in MVSMC of type 2 diabetic mice. There was increased expression of miR-125b as well as key inflammatory genes in MVSMC derived from *db/db* mice relative to control *db/+* mice, and both these increases persisted even after culturing the MVSMC for several passages in vitro, possibly due to "metabolic memory" in this type 2 diabetic mouse model. In addition, immunoblotting of cell lysates and immunohistochemistry of aortic sections showed a decrease in Suv39h1 K9 HMT in diabetic *db/db* mice relative to *db/+*. We recently showed that decreased Suv39h1 in *db/db* MVSMC can play a role, at least in part, in the increased expression of inflammatory genes in these cells (22). Interestingly, we now found that Suv39h1 is a target of miR-125b, and

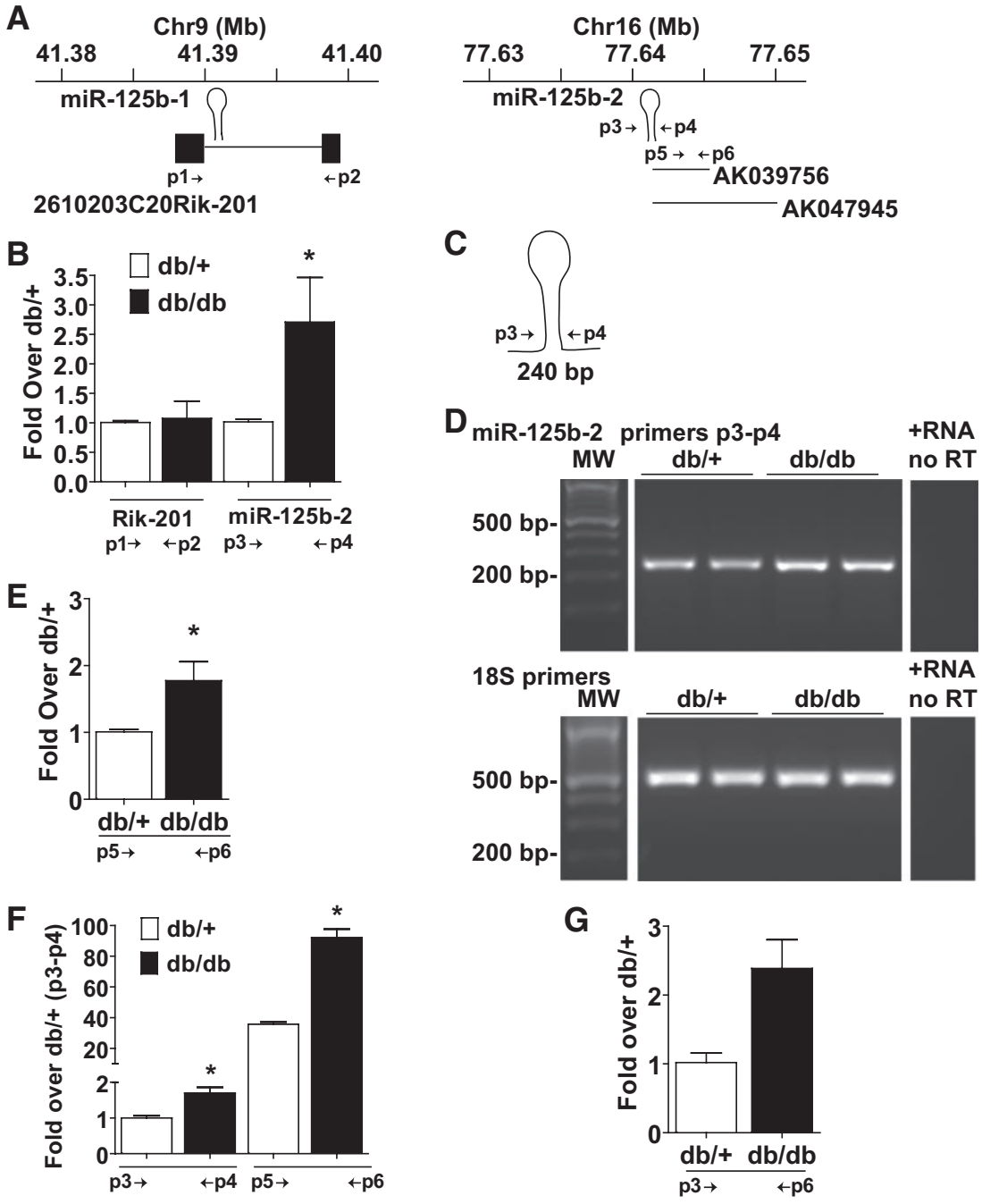

FIG. 6. Increased transcriptional regulation of miR-125b-2 in *db/db* MVSMC. *A*: Chromosomal map of the genomic locations of miR-125b isoforms, as well as two RIKEN cDNA clones that overlap miR-125b-2 along with primer locations designated as *numbered arrowheads*. *B–G*: Total RNA was extracted from MVSMC followed by RT-PCRs. *B*: RT-qPCRs using primers p1–p2 for 2610203C20Rik-201 (Rik-201) or primers p3–p4 flanking the premiR-125b-2 sequence. Results expressed as fold over *db/+* (*$P < 0.05$ vs. *db/+*, $n = 6$). *C* and *D*: Using conventional PCR and gel electrophoresis with primers flanking the premiR-125b-2 on chromosome 16 (primers p3–p4), an unprocessed premiR-125b-2 would result in a 240 bp fragment. *D*: Primers p3–p4 reveal a 240-bp fragment which is increased in *db/db* relative to *db/+* VSMC. As a negative control, an RNA sample with no reverse transcriptase (no RT) was used for conventional PCR to demonstrate the absence of contamination of genomic DNA in the RNA used for RT-PCR. As an internal control in conventional PCR, 18S primers were used. Contrast of the gel was adjusted uniformly across the whole gel to better visualize the bands. *E*: RT-qPCR of transcript levels downstream of premiR-125b-2 overlapping RIKEN cDNA clones using primers p5–p6. Results are expressed as fold over *db/+* (*$P < 0.05$ vs. *db/+*, $n = 5$). *F*: Representative results of overall cDNA transcript levels relative to *db/+* amplified with primers p3–p4 (*$P < 0.05$ vs. *db/+* within each primer set, primers p3–p4, $n = 6$, and primers p5–p6, $n = 5$). *G*: RT-qPCR amplification of transcript containing both miR-125b-2 and the downstream cDNA using primers p3–p6. Results from one experiment performed in triplicate.

that increased miR-125b can subsequently decrease H3K9me3 repressive marks at inflammatory gene promoters, leading to a corresponding increase in expression of inflammatory genes such as *IL-6* and *MCP-1*. The miR-125b mimic specifically downregulated H3K9me3, but not H3K9me2 and H3K9me1. Furthermore, increasing miR-125b levels (with miR-125b mimic) in control *db/+* MVSMC functionally led to increased monocyte-MVSMC binding, mimicking the diabetic phenotype. Since miR-125b could mimic key diabetic phenotypes, aberrant regulation of miR-125b may be an underlying mechanism for sustained vascular dysfunction, at least

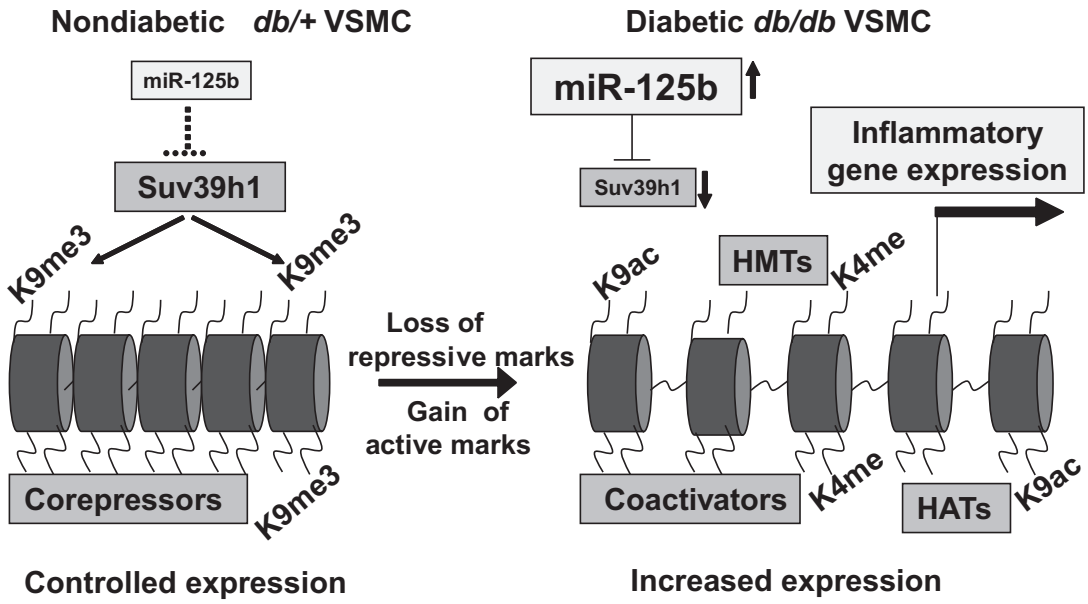

FIG. 7. Model for the mechanisms related to miR-125b mediated decrease in SUV39H1, leading to loss of repression of inflammation in diabetic VSMC. Diabetic conditions in the *db/db* VSMC can promote the decrease of Suv39h1 (via increased miR-125b) and concomitant loss of repressive chromatin marks such as H3K9 trimethylation (K9me3) relative to nondiabetic *db*+ cells. This can lead to a more open chromatin state (right) characterized by active chromatin marks such as K4methylation (K4me) and related HMTs, K9acetylation (K9ac) and related coactivators and histone acetyl transferases (HATs) generally associated with active gene expression. Together such events can result in increased expression of inflammatory genes. Various combinations of histone modifications are likely to be involved.

in this type 2 diabetic model, by targeting and downregulating a key chromatin HMT that normally keeps key inflammatory genes in the repressed state (Fig. 7). Additional histone modifications, such as H3K4-acetylation and H3K4me activating marks, as suggested in previous studies (24–25,43), and/or key histone demethylases, may also cooperate to orchestrate dynamic events at these gene promoters along with this miR-mediated loss of repression to promote chronic vascular inflammation and accelerated atherosclerosis seen in diabetes (Fig. 7).

It has been reported that miR-125b targets p53 in neuroblastoma and lung fibroblast cells, effectively inhibiting apoptosis (44), whereas p53 was upregulated in adipose tissue of type 2 diabetic mice and correlated with increased oxidant stress, inflammation, and insulin resistance (45). However, miR-125b levels in adipose tissue were not evaluated. Additionally, a recent report in leukemia cells did not identify p53 as a miR-125b target (46). Thus, there may be cell-specific targeting of p53 by miR-125b. It is unclear whether miR-125b plays a role in p53 regulation in diabetic VSMC. Although such p53-dependent mechanisms could regulate the increased hypertrophy and proliferation of diabetic VSMC, they are beyond the scope of this study.

In neural cells, miR-125b was upregulated by reactive oxygen species (47), and via NF-κB-dependent mechanisms by TNF-α in macrophages and human cholangiocyte cells (48–49). Increased inflammatory genes in diabetes and *db/db* vasculature have been attributed, at least in part, to increased oxidant stress (50), which is also implicated in metabolic memory and activation of the proinflammatory transcription factor NF-κB (3,6,17,24,51). Thus, miR-125b might be regulated by oxidant stress and proinflammatory stimuli under diabetic conditions, which could target Suv39h1, leading to decreased H3K9me3 and subsequent upregulation of inflammatory genes associated with diabetic complications. This vicious cycle may explain the sustained expression of inflammatory genes in diabetic *db/db* cells, even after in vitro culture where the aberrant upregulation of miR-125b may contribute to persistent vascular inflammation by targeting and suppressing a crucial HMT which maintains key genes in a controlled or repressed state.

Interestingly, high glucose could decrease inflammatory gene promoter H3K9me3 in human VSMC and endothelial cells (22,25), and increased expression of miR-125a (related to miR-125b) was observed in several tissues of GK type 2 diabetic rats (52). However, it is not yet clear whether high glucose can directly increase miR-125b or decrease SUV39H1 protein levels. Other factors, including altered Suv39h1 occupancy and/or H3K9 demethylases, may also be involved in high glucose-induced decrease in H3K9 methylation in VSMC. The mechanisms responsible for the increased miR-125b in *db/db* MVSMC may be quite complex, involving other factors related to type 2 diabetic or insulin resistance in the *db/db* mice besides hyperglycemia. Additional work is needed to explore these aspects and to determine whether miR-125b levels are reversed after glycemic control in diabetic mice, and whether miR-125b plays any role in metabolic memory.

The mechanisms by which miRs themselves are regulated and expressed under normal or disease conditions are currently of great interest. Our results suggest that the increase in miR-125b is likely caused by increased transcription of miR-125b-2. We identified two RIKEN cDNAs partially overlapping with miR-125b-2, and RT-qPCR could amplify a transcript covering this region. Our data indicate that the cellular machinery may transcribe this region as one transcript which then undergoes miR processing to remove the 5′end containing miR-125b-2 for majority of the transcripts, whereas the remaining RIKEN cDNA clone is more stable and maintains an as yet unknown function. A potential promoter region for miR-125b-2 and the RIKEN cDNAs was not easily identifiable based on sequence alone and remains an interesting area of future research. In

addition, regulation at the level of miR processing of either copy of miR-125b cannot be ruled out. It is also not fully clear how miR-125b or its promoter is regulated under diabetic conditions, why it continues to remain elevated in the diabetic cells even after culture in vitro, and if this increase in miR-125b is caused by dysregulated chromatin in the diabetic state or vice versa.

In summary, these results provide new insights into the cross-talk and relationships between miRs and epigenetic histone lysine methylation leading to inflammatory gene expression in VSMC, especially in a disease relevant model related to diabetic vascular inflammation. Although miR-125b has been implicated in various cancers (28,53), this is the first indication of a role in vascular complications of diabetes. Given the exciting advances in the development of miR inhibitors, such as antagomirs and locked nucleic acid modified small RNAs (54), anti-miR–based therapies could potentially be developed for diabetic complications and other inflammatory diseases.

ACKNOWLEDGMENTS

This work was supported by grants from the National Institutes of Health (the National Heart, Lung and Blood Institute and the National Institute of Diabetes and Digestive and Kidney Diseases) (to R.N.), predoctoral fellowships from the Myrtle Carr Foundation and City of Hope's Irell and Manella Graduate School of Biological Sciences (to L.M.V.), and a Junior Faculty Award from the American Diabetes Association (to M.A.R.).

No potential conflicts of interest relevant to this article were reported.

L.M.V., M.K., M.A.R., and R.N. researched data, contributed to discussion, wrote, reviewed, and edited the manuscript. M.W. and L.L researched data.

The authors thank Drs. Ivan Todorov, Laura Arce, and Ali Ehsani and Sofia Loera, Beckman Research Institute of City of Hope, for all their help, and also those who generously provided plasmid vectors.

REFERENCES

1. Libby P, Ridker PM, Maseri A. Inflammation and atherosclerosis. Circulation 2002;105:1135–1143
2. Devaraj S, Dasu MR, Jialal I. Diabetes is a proinflammatory state: a translational perspective. Expert Rev Endocrinol Metab 2010;5:19–28
3. Brownlee M. Biochemistry and molecular cell biology of diabetic complications. Nature 2001;414:813–820
4. Dandona P, Aljada A, Bandyopadhyay A. Inflammation: the link between insulin resistance, obesity and diabetes. Trends Immunol 2004;25:4–7
5. Guha M, Bai W, Nadler JL, Natarajan R. Molecular mechanisms of tumor necrosis factor α gene expression in monocytic cells via hyperglycemia-induced oxidant stress-dependent and -independent pathways. J Biol Chem 2000;275:17728–17739
6. Yerneni KK, Bai W, Khan BV, Medford RM, Natarajan R. Hyperglycemia-induced activation of nuclear transcription factor κB in vascular smooth muscle cells. Diabetes 1999;48:855–864
7. Libby P, Plutzky J. Diabetic macrovascular disease: the glucose paradox? Circulation 2002;106:2760–2763
8. King GL, Das-Evcimen D: Role of protein kinase C in diabetic complications. Expert Rev. Endocrinol Metab 2010;5:77–88
9. Yan SF, Ramasamy R, Schmidt AM. Receptor for AGE (RAGE) and its ligands-cast into leading roles in diabetes and the inflammatory response. J Mol Med 2009;87:235–247
10. Shanmugam N, Reddy MA, Guha M, Natarajan R. High glucose-induced expression of proinflammatory cytokine and chemokine genes in monocytic cells. Diabetes 2003;52:1256–1264
11. Glass CK, Witztum JL. Atherosclerosis. the road ahead. Cell 2001;104:503–516
12. Martin C, Zhang Y. The diverse functions of histone lysine methylation. Nat Rev Mol Cell Biol 2005;6:838–849
13. Peters AH, Kubicek S, Mechtler K, O'Sullivan RJ, Derijck AA, Perez-Burgos L, Kohlmaier A, Opravil S, Tachibana M, Shinkai Y, Martens JH, Jenuwein T. Partitioning and plasticity of repressive histone methylation states in mammalian chromatin. Mol Cell 2003;12:1577–1589
14. Mal AK. Histone methyltransferase Suv39h1 represses MyoD-stimulated myogenic differentiation. Embo J 2006;25:3323–3334
15. El Gazzar M, Yoza BK, Hu JY, Cousart SL, McCall CE. Epigenetic silencing of tumor necrosis factor α during endotoxin tolerance. J Biol Chem 2007;282:26857–26864
16. Saccani S, Natoli G. Dynamic changes in histone H3 Lys 9 methylation occurring at tightly regulated inducible inflammatory genes. Genes Dev 2002;16:2219–2224
17. Ihnat MA, Thorpe JE, Ceriello A. Hypothesis: the 'metabolic memory', the new challenge of diabetes. Diabet Med 2007;24:582–586
18. Nathan DM, Cleary PA, Backlund JY, Genuth SM, Lachin JM, Orchard TJ, Raskin P, Zinman B. Intensive diabetes treatment and cardiovascular disease in patients with type 1 diabetes. N Engl J Med 2005;353:2643–2653
19. Colagiuri S, Cull CA, Holman RR. Are lower fasting plasma glucose levels at diagnosis of type 2 diabetes associated with improved outcomes?: U.K. prospective diabetes study 61. Diabetes Care 2002;25:1410–1417
20. Holman RR, Paul SK, Bethel MA, Matthews DR, Neil HA. 10-year follow-up of intensive glucose control in type 2 diabetes. N Engl J Med 2008;359:1577–1589
21. Li SL, Reddy MA, Cai Q, Meng L, Yuan H, Lanting L, Natarajan R. Enhanced proatherogenic responses in macrophages and vascular smooth muscle cells derived from diabetic db/db mice. Diabetes 2006;55:2611–2619
22. Villeneuve LM, Reddy MA, Lanting LL, Wang M, Meng L, Natarajan R. Epigenetic histone H3 lysine 9 methylation in metabolic memory and inflammatory phenotype of vascular smooth muscle cells in diabetes. Proc Natl Acad Sci U S A 2008;105:9047–9052
23. Miao F, Wu X, Zhang L, Yuan YC, Riggs AD, Natarajan R. Genome-wide analysis of histone lysine methylation variations caused by diabetic conditions in human monocytes. J Biol Chem 2007;282:13854–13863
24. El-Osta A, Brasacchio D, Yao D, Pocai A, Jones PL, Roeder RG, Cooper ME, Brownlee M. Transient high glucose causes persistent epigenetic changes and altered gene expression during subsequent normoglycemia. J Exp Med 2008;205:2409–2417
25. Brasacchio D, Okabe J, Tikellis C, Balcerczyk A, George P, Baker EK, Calkin AC, Brownlee M, Cooper ME, El-Osta A. Hyperglycemia induces a dynamic cooperativity of histone methylase and demethylase enzymes associated with gene-activating epigenetic marks that coexist on the lysine tail. Diabetes 2009;58:1229–1236
26. Kim VN, Han J, Siomi MC. Biogenesis of small RNAs in animals. Nat Rev Mol Cell Biol 2009;10:126–139
27. Bartel DP. MicroRNAs: target recognition and regulatory functions. Cell 2009;136:215–233
28. Esquela-Kerscher A, Slack FJ. Oncomirs—microRNAs with a role in cancer. Nat Rev Cancer 2006;6:259–269
29. Poy MN, Eliasson L, Krutzfeldt J, Kuwajima S, Ma X, Macdonald PE, Pfeffer S, Tuschl T, Rajewsky N, Rorsman P, Stoffel M. A pancreatic islet-specific microRNA regulates insulin secretion. Nature 2004;432:226–230
30. Cordes KR, Sheehy NT, White MP, Berry EC, Morton SU, Muth AN, Lee TH, Miano JM, Ivey KN, Srivastava D. miR-145 and miR-143 regulate smooth muscle cell fate and plasticity. Nature 2009;460:705–710
31. Ji R, Cheng Y, Yue J, Yang J, Liu X, Chen H, Dean DB, Zhang C. MicroRNA expression signature and antisense-mediated depletion reveal an essential role of MicroRNA in vascular neointimal lesion formation. Circ Res 2007;100:1579–1588
32. Lin Y, Liu X, Cheng Y, Yang J, Huo Y, Zhang C. Involvement of MicroRNAs in hydrogen peroxide-mediated gene regulation and cellular injury response in vascular smooth muscle cells. J Biol Chem 2009;284:7903–7913
33. Liu X, Cheng Y, Zhang S, Lin Y, Yang J, Zhang C. A necessary role of miR-221 and miR-222 in vascular smooth muscle cell proliferation and neointimal hyperplasia. Circ Res 2009;104:476–487
34. Xin M, Small EM, Sutherland LB, Qi X, McAnally J, Plato CF, Richardson JA, Bassel-Duby R, Olson EN. MicroRNAs miR-143 and miR-145 modulate cytoskeletal dynamics and responsiveness of smooth muscle cells to injury. Genes Dev 2009;23:2166–2178
35. Wang Q, Wang Y, Minto AW, Wang J, Shi Q, Li X, Quigg RJ. MicroRNA-377 is up-regulated and can lead to increased fibronectin production in diabetic nephropathy. FASEB J 2008;22:4126–4135
36. Kato M, Arce L, Natarajan R. MicroRNAs and their role in progressive kidney diseases. Clin J Am Soc Nephrol 2009;4:1255–1266
37. Kato M, Putta S, Wang M, Yuan H, Lanting L, Nair I, Gunn A, Nakagawa Y, Shimano H, Todorov I, Rossi JJ, Natarajan R. TGF-β activates Akt kinase through a microRNA-dependent amplifying circuit targeting PTEN. Nat Cell Biol 2009;11:881–889

38. Kato M, Zhang J, Wang M, Lanting L, Yuan H, Rossi JJ, Natarajan R. MicroRNA-192 in diabetic kidney glomeruli and its function in TGF-β-induced collagen expression via inhibition of E-box repressors. Proc Natl Acad Sci U S A 2007;104:3432–3437
39. Wong CF, Tellam RL. MicroRNA-26a targets the histone methyltransferase Enhancer of Zeste homolog 2 during myogenesis. J Biol Chem 2008;283:9836–9843
40. Reddy MA, Li SL, Sahar S, Kim YS, Xu ZG, Lanting L, Natarajan R. Key role of Src kinase in S100B-induced activation of the receptor for advanced glycation end products in vascular smooth muscle cells. J Biol Chem 2006;281:13685–13693
41. Doran AC, Meller N, McNamara CA. Role of smooth muscle cells in the initiation and early progression of atherosclerosis. Arterioscler Thromb Vasc Biol 2008;28:812–819
42. Cai Q, Lanting L, Natarajan R. Interaction of monocytes with vascular smooth muscle cells regulates monocyte survival and differentiation through distinct pathways. Arterioscler Thromb Vasc Biol 2004;24:2263–2270
43. Li Y, Reddy MA, Miao F, Shanmugam N, Yee JK, Hawkins D, Ren B, Natarajan R. Role of the histone H3 lysine 4 methyltransferase, SET7/9, in the regulation of NF-κB-dependent inflammatory genes. Relevance to diabetes and inflammation. J Biol Chem 2008;283:26771–26781
44. Le MT, Teh C, Shyh-Chang N, Xie H, Zhou B, Korzh V, Lodish HF, Lim B. MicroRNA-125b is a novel negative regulator of p53. Genes Dev 2009;23:862–876
45. Minamino T, Orimo M, Shimizu I, Kunieda T, Yokoyama M, Ito T, Nojima A, Nabetani A, Oike Y, Matsubara H, Ishikawa F, Komuro I. A crucial role for adipose tissue p53 in the regulation of insulin resistance. Nat Med 2009;15:1082–1087
46. Klusmann JH, Li Z, Bohmer K, Maroz A, Koch ML, Emmrich S, Godinho FJ, Orkin SH, Reinhardt D. miR-125b-2 is a potential oncomiR on human chromosome 21 in megakaryoblastic leukemia. Genes Dev 2010;24:478–490
47. Lukiw WJ, Pogue AI. Induction of specific micro RNA (miRNA) species by ROS-generating metal sulfates in primary human brain cells. J Inorg Biochem 2007;101:1265–1269
48. Tili E, Michaille JJ, Cimino A, Costinean S, Dumitru CD, Adair B, Fabbri M, Alder H, Liu CG, Calin GA, Croce CM. Modulation of miR-155 and miR-125b levels following lipopolysaccharide/TNF-α stimulation and their possible roles in regulating the response to endotoxin shock. J Immunol 2007;179:5082–5089
49. Zhou R, Hu G, Liu J, Gong AY, Drescher KM, Chen XM: NF-kappaB p65-dependent transactivation of miRNA genes following cryptosporidium parvum infection stimulates epithelial cell immune responses. PLoS Pathog 2009;5:e1000681
50. San Martin A, Du P, Dikalova A, Lassegue B, Aleman M, Gongora MC, Brown K, Joseph G, Harrison DG, Taylor WR, Jo H, Griendling KK. Reactive oxygen species-selective regulation of aortic inflammatory gene expression in type 2 diabetes. Am J Physiol Heart Circ Physiol 2007;292:H2073–2082
51. Bierhaus A, Schiekofer S, Schwaninger M, Andrassy M, Humpert PM, Chen J, Hong M, Luther T, Henle T, Kloting I, Morcos M, Hofmann M, Tritschler H, Weigle B, Kasper M, Smith M, Perry G, Schmidt AM, Stern DM, Haring HU, Schleicher E, Nawroth PP. Diabetes-associated sustained activation of the transcription factor nuclear factor-κB. Diabetes 2001;50:2792–2808
52. Herrera BM, Lockstone HE, Taylor JM, Wills QF, Kaisaki PJ, Barrett A, Camps C, Fernandez C, Ragoussis J, Gauguier D, McCarthy MI, Lindgren CM. MicroRNA-125a is over-expressed in insulin target tissues in a spontaneous rat model of type 2 diabetes. BMC Med Genomics 2009;2:54
53. Bousquet M, Quelen C, Rosati R, Mansat-De Mas V, La Starza R, Bastard C, Lippert E, Talmant P, Lafage-Pochitaloff M, Leroux D, Gervais C, Viguie F, Lai JL, Terre C, Beverlo B, Sambani C, Hagemeijer A, Marynen P, Delsol G, Dastugue N, Mecucci C, Brousset P. Myeloid cell differentiation arrest by miR-125b-1 in myelodysplastic syndrome and acute myeloid leukemia with the t(2,11)(p21;q23) translocation. J Exp Med 2008;205:2499–2506
54. Soifer HS, Rossi JJ, Saetrom P. MicroRNAs in disease and potential therapeutic applications. Mol Ther 2007;15:2070–2079